Deep Mining 2024 – P Andrieux & D Cumming-Potvin (eds)

doi:10.36487/ACG_repo/2465_35

Investigating energy dissipation and deformation capacity of ground support schemes under dynamic loading: results from LaRonde and Kittilä mines' drop test program

Christopher Durham [a,*], **Véronique Falmagne** [a], **Marie-Eve Caron** [a], **Antti Pyy** [b], **Rico Brändle** [c]

[a] *Agnico Eagle Mines, Canada*

[b] *Agnico Eagle Mines, Finland*

[c] *Geobrugg AG, Switzerland*

Abstract

Over the past decade, mining-induced seismicity and the consequences of dynamic loading on ground support schemes have become a focus of ground control management and one of the major challenges at LaRonde mine, as it extends below 3,000 m. The Kittilä mine manages high deformation in some areas and is experiencing dynamic conditions at depth. In some rare occurrences, dynamic loading from seismic events have exceeded the capacity of ground support schemes at both sites. Furthermore, the ground control practices implemented to safely manage seismic conditions in development drives have been largely successful, but introduce operational efficiency and cost challenges. Thus as the mines progress deeper there is a need to implement ground support schemes that are not only tougher but also more efficient to install, considering current practices and available equipment at each operation. In line with a process of continuous improvement, a dynamic drop testing program was initiated at Geobrugg's facility in Walenstadt, Switzerland, in collaboration with Geobrugg, LaRonde and Kittilä mines, to study the performance of various ground support schemes for both sites.

This paper details the experimental program and the results of tests with a comparative analysis of the tested schemes. This large-scale laboratory testing program and the detailed analysis process of the conducted drop tests enable better understanding of the dynamic behaviour of different configurations of ground support schemes using the products currently employed at both mines, and help to identify possible avenues for improving the ground support scheme. The testing program is intended to guide improvements in the design of ground support schemes for deep mining conditions.

Keywords: *deep mining, seismicity, dynamic ground support schemes, dynamic testing, rockburst, high stress*

1 Introduction

Deep underground mining environments present unique challenges for the design of ground support schemes, particularly in zones susceptible to squeezing, stress-induced rock failure and rockbursting. Ground support schemes designed primarily to control gravity-induced rockfalls in blocky rock masses have been found to be unsuitable for such environments. Terminology proposed by Windsor & Thompson (1992), as presented in Villaescusa et al. (2023), is used for consistency. Hence, a 'ground support scheme' is defined as a combination of surface support system (plates, mesh, straps, liner or shotcrete) and a reinforcement system (rockbolts and cable bolts). Dynamic conditions require ground support schemes to comply with energy dissipation requirements and sustain rapid rock mass deformation. It is also essential that the load

* Corresponding author. Email address: christopher.durham@agnicoeagle.com

and deformation characteristics of the ground support elements be compatible with one another to ensure optimal load transfer from the rock mass to the reinforcement and surface support.

The LaRonde and Kittilä mines have independently developed control measures and ground support design and installation strategies that are best suited to their respective environments (refer to Sasseville et al. 2022 for LaRonde mine). The purpose of the collaborative study was to examine the relative performance of different ground support elements in the spirit of continuous improvement of ground support schemes at each mine.

2 Background

While the concept of using yielding bolts to mitigate dynamic rock mass failure was established early on (Ortlepp & Stacey 1994), significant advancements have been made in developing reinforcement and support elements with combined energy absorption and displacement capabilities. Extensive laboratory and field testing, both static and dynamic, have been conducted on individual elements (e.g. bolts, mesh, shotcrete) and their combinations (Brändle et al. 2019; Doucet & Voyzelle 2012; Potvin & Hadjigeorgiou 2020; Kaiser et al. 1996; Knox & Hadjigeorgiou 2022; Villaescusa et al. 2023). These researchers have provided valuable technical specifications, performance data and insights into the behaviour of individual components.

However, assessing the performance of complete ground support schemes, where multiple elements interact under dynamic loading, requires large-scale laboratory testing facilities like the one established by Geobrugg in Walenstadt, Switzerland (Brändle et al. 2017; Roth et al. 2014; Vallejos et al. 2019).

As LaRonde is extending mining under high-stress conditions below 3,260 m, continuous improvement of the ground support scheme is a priority. Given the wide range of available ground support products, a large-scale laboratory testing program was collaboratively developed with Geobrugg and the LaRonde and Kittilä mines. This program aims to better understand the dynamic behaviour and energy dissipation capacity of various support scheme configurations using products currently employed at both mines; ultimately identifying potential improvements for ground support strategies.

A detailed description of the motivation for the study, an overview of the test site and set-up, and the testing and results analysis methodology are extensively detailed in Durham et al. (2024). Essentially, for all the test configurations conducted in this drop testing program, a block weighing 6,280 kg was elevated to a drop height of 1.59 m using a crane. A potential energy at impact was standardised at 98 kJ to challenge the system's limits and potentially induce failure. After impact, as the block travels down, the gravitational force continues to act on the block while the ground support scheme exerts an opposite force to retain it. The latter represents the energy dissipated by the ground support scheme. An instrumentation set-up comprising a high-speed camera, accelerometers and load cells was used to measure block motion and energy dissipation by the ground support scheme during impact.

Durham et al. (2024), described the results of three test configurations: LR1, LR2 and LR3. The materials for the tests and design configurations were provided by each mine and representatives attended most of the tests. The detailed analysis of these three tests, presented in Durham et al. (2024), revealed that dynamic bolts paired with well-matched plates optimise energy dissipation, thereby reducing the load and dependency on the surface support system. The experiments also highlight the superior performance of high-tensile-strength woven mesh over traditional welded wire mesh, due to its efficient load distribution and energy absorption capabilities. The results and analyses of the last three tests for LaRonde (LR4 to 6) and one test for Kittilä (KI1) are detailed in the following sections.

Efforts were made to maintain consistency between tests and avoid varying several parameters at the same time. Nonetheless, unlike the first three tests, which were all conducted on the same rig (rig 1), the tests described in the next section were conducted on both rigs 1 and 2.

Finally, as indicated in Durham et al. (2024), the testing was done using split tubes for the central bolt when these were either PAR1 (Epiroc 2024) or D-Bolt (Normet 2024). The location of the split was selected to coincide with the smooth debonded portion of these bolts. When the central bolt was a rebar, a continuous tube was used.

3 Dynamic testing program

A total of seven configurations were tested as part of the entire study. Configurations LR1 to LR6 were tested using ground support material from LaRonde mine, whereas configuration KI1 was tested using material from Kittilä mine. This section details each configuration.

3.1 Configurations LR1, LR2, LR3

Configurations LR1, LR2 and LR3, listed in Table 1, were detailed in Durham et al. (2024), therefore only key common elements are repeated here:

- They are tested on rig 1.
- The pattern for reinforcement elements is 1.4 by 1.4 m with a centre bolt. This pattern differs from the one used at LaRonde mine (1.2 by 1.2 m with a centre bolt). Since bolt positions were limited on rig 1, the selected pattern allows for comparability of the results on both rigs.
- To prevent excessive lateral displacement of the peripheral bolts during impact, empty steel tubes were attached to them.
- No shotcrete was used with these configurations.
- Reinforcement elements were resin-grouted as per specifications.
- Ground support material was provided by LaRonde mine.

Table 1 Summary of configurations LR1, LR2 and LR3

Test ID	LR1	LR2	LR3
Mesh system type	Welded wire mesh, gauge #4	Minax, 80/4.6 mm	Minax 80/4.6 mm
Centre bolt (F5)	Rebar, 22 mm	Rebar, 22 mm	PAR1, 22 mm
Bolt plate	10-ton dome	10-ton dome	21-ton dome
Split tube	No	No	Yes

3.2 Configurations LR4, LR5, LR6 and KI1

The test set-ups from configurations LR4, LR5, LR6 and KI1 are extensively detailed in this section and briefly detailed in Table 2. Figure 1 presents the configurations for the reinforcement and support systems used in each test.

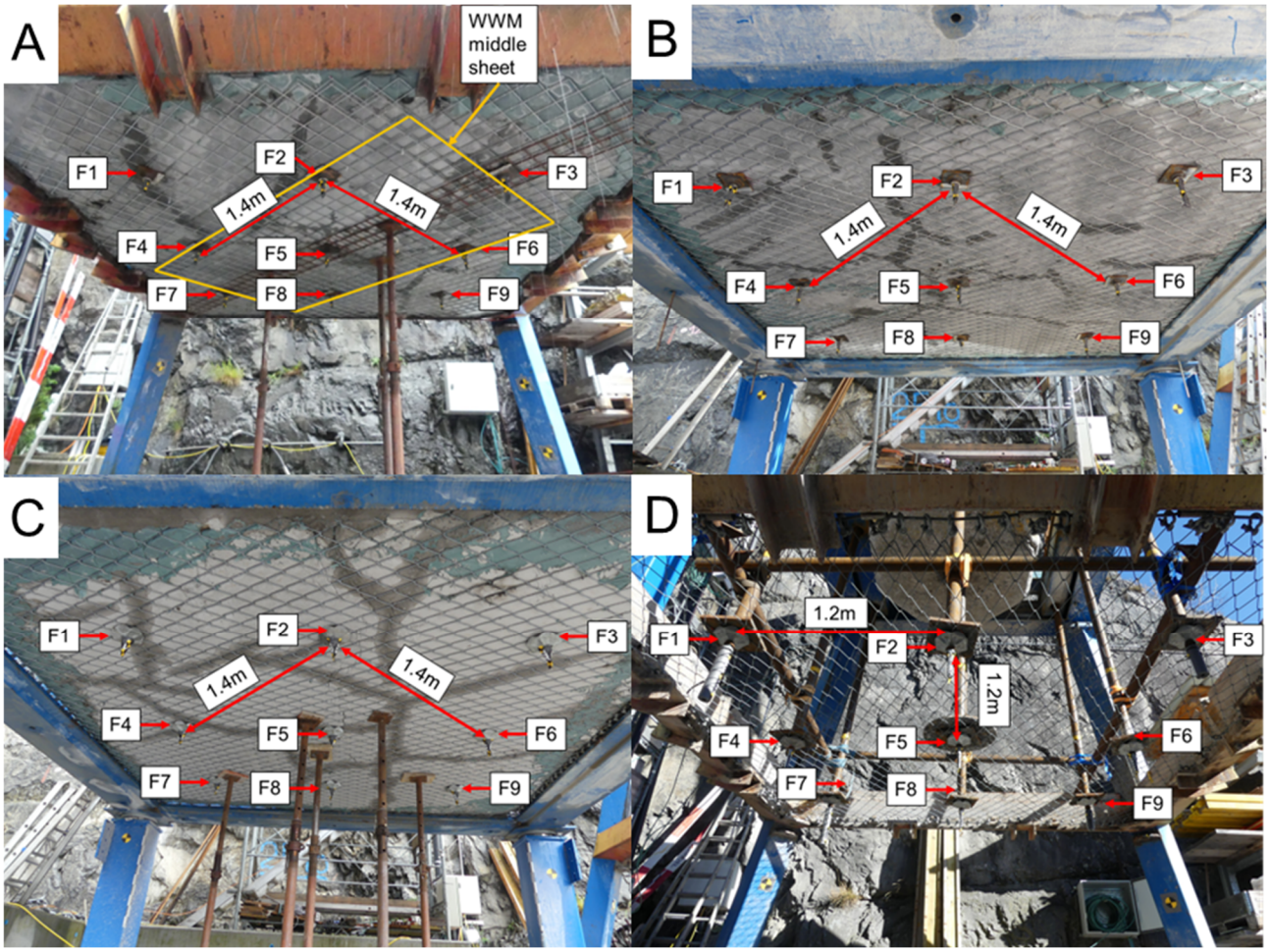

Figure 1 Overview of the testing configurations from the underside before impact: (a) LR4; (b) LR5; (c) LR6; (d) KI1. The bolt numbering system is consistent for each test

3.2.1 Configuration LR4

Testing configuration LR4 was performed on rig 1. In this set-up the reinforcement system consisted of a middle bolt (F5) and a 22 mm 6'2" resin-grouted rebar in a continuous tube with a 10-ton dome plate and a rebar dome nut. The peripheral bolts were yielding bolts (PAR1, EPIROC 2024), 22 mm, 7' grouted with resin, a 21-ton dome plate, a dome nut and continuous tubes. The bolting pattern was 1.4 by 1.4 m, with a centre bolt (F5).

For the surface support system, the welded wire mesh (WWM) used was gauge #4, with 4" by 4" squares, in sheets of 5' by 9'. A mesh strap, gauge #0 and 16' long, provided by Kittilä mine, was installed diagonally as recommended. The middle mesh sheet was anchored by bolts F2, F4, F5 (middle), F6 and F8 through the last square of the mesh, differing from the standard three-square overlap due to the modified bolt spacing, which was addressed and discussed in Durham et al. (2024).

A 10 cm layer of steel-fibre-reinforced shotcrete was poured over plastic wrap on the mesh to prevent adherence or pouring through the mesh. This shotcrete layer was mixed at the test site using material specifications provided by Kittilä. The layer differs in thickness, fibre density and its installation method (not sprayed) compared to LaRonde practices. Nonetheless, the shotcrete layer was constructed in a similar fashion for all the tests designed with shotcrete and the tests are therefore comparable despite the lack of installation control by the mine representatives and the difference with underground applications. No empty steel tubes were needed to fix the peripheral bolts as the shotcrete layer prevented lateral displacement.

3.2.2 Configuration LR5

Configuration LR5 was the first test to be performed on rig 2, as shown in Figure 1b. The reinforcement system consists of a middle bolt F5, a 22 mm, 6’2” rebar with resin, a 10-ton dome plate, a rebar dome nut and a continuous tube. The peripheral bolts are yielding (PAR1, EPIROC 2024) 22 mm, 7’ with resin, a 21-ton dome plate, a dome nut and continuous tubes. The bolting pattern is 1.4 by 1.4 m, with a centre bolt (F5).

The surface support system consisted of Minax 80/4.6 mm (M8046) mesh. Additionally, a 10 cm layer of fibre-reinforced shotcrete was applied, with the same description and installation technique as for LR4. The main differences between configurations LR4 and LR5 are the use of rig 2 and the replacement of the mesh and mesh strap with Minax M8046.

3.2.3 Configuration LR6

Configuration LR6 is similar to LR5 and it was also tested on rig 2. The ground support system consists of the same reinforcement and surface elements, except for the use of G-Plates (Geobrugg 2013) instead of a regular 10-ton dome plate.

3.2.4 Configuration KI1

Configuration KI1 uses ground support materials from Kittilä mine. The reinforcement system consists of a middle bolt F5, a 22 mm, 2.4 m D-Bolt (Normet 2024) with cement grout in a split tube and a G-Plate. A square steel plate was added behind the mesh to ensure load transfer to the centre bolt. The peripheral bolts are also 22 mm, 2.4 m D-Bolts with cement grout, G-Plates and split tubes. The bolting pattern is 1.2 by 1.2 m, with no centre bolt. The surface support system is Minax 80/4 mm (M8040) mesh. No shotcrete layer was placed above the mesh so steel tubes were attached to the peripheral bolts to prevent lateral displacements, as in tests LR1 to 3.

4 Analysis of results

For each tested configuration detailed in the previous section a thorough analysis was conducted using comprehensive data analysis and video interpretation. The analysis methodology, detailed in Durham et al. (2024), provides a consistent framework for describing the behaviour and response to dynamic loading of each testing configuration. The limitations of each tested configuration are identified. This approach ensures that the observed outcomes accurately align with the recorded data. The analysis results for test configurations LR4, LR5, LR6 and KI1 are presented in this section.

4.1 Configuration LR4

This subsection presents the analysis of the results derived from dynamic testing of the LR4 configuration. In this configuration, a 10 cm layer of poured steel-fibre-reinforced shotcrete covers the surface support system, which consists of #4 gauge WWM sheets with a #0 gauge mesh strap linked by peripheral bolts F3 and F7. The reinforcement system includes the central bolt F5 and a 22 mm rebar with a 10-ton dome plate in a continuous tube.

Figure 2a presents a graph of the block’s displacement and energy dissipation versus time in milliseconds. Time zero in all graphs is when the block touches the ground support, i.e. at impact. Figure 2b shows the block’s acceleration and variations in velocity after impact. Figure 2c records the load on each bolt. Together the graphs provide insight into the behaviour of individual reinforcement elements and the scheme’s overall capacity to absorb and redistribute dynamic loads. In Figure 2 and in all subsequent results presented thereafter, key steps in the progressive failure process are marked by vertical lines at specific time intervals, defining the phases of failure as described below.

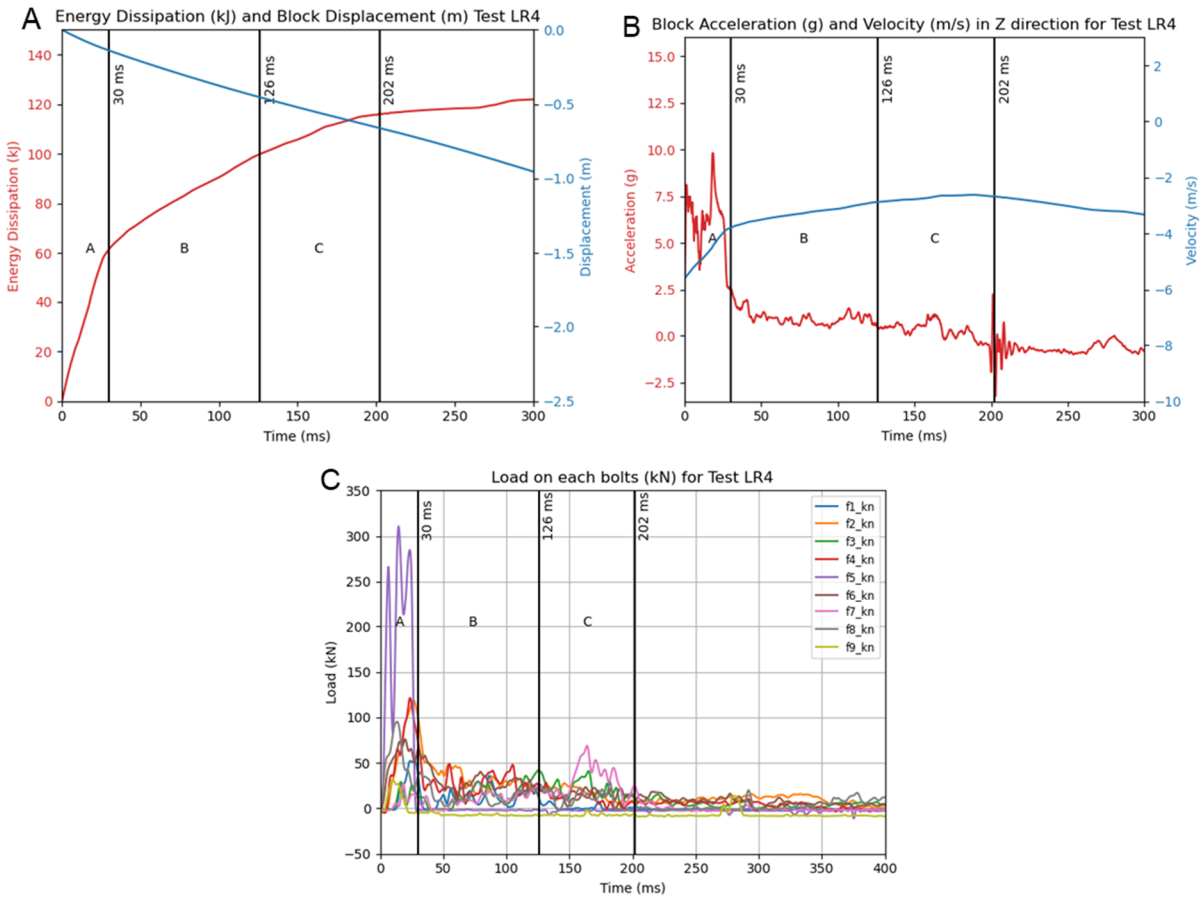

Figure 2 Results and data visualisation for testing configuration LR4: (a) Block displacement (m) and energy dissipation during impact; (b) Block acceleration (g) and velocity (m/s) during impact; (c) Bolt load distribution during impact

The breakdown of the failure process for configuration LR4 is detailed as follows.

4.1.1 Phase A (0 to 30 ms): initial impact, shotcrete layer fracture propagation and reinforcement system response

The block initially impacts the shotcrete layer, causing a rapid deceleration before fracture propagation occurs and results in shotcrete block formations of various sizes and dimensions. This allows the falling block to transfer the load to the reinforcement system, specifically the centre bolt F5. In this test the plate effectively transfers the load to the bolt, which deforms and eventually fails at the threads.

Among all the tested configurations where the centre bolt F5 consists of a 22 mm resin-grouted rebar with a 10-ton dome plate (tests LR1, LR2, LR4, and LR5), only test LR4 successfully transferred the load to cause bolt failure. In contrast, tests LR1, LR2 (Durham et al. 2024) and LR5 showed plate failure, whereas in LR4 the centre bolt reached failure.

This outcome in test LR4 might be attributed to the irregular fracture propagation of the shotcrete around the falling block, as shown in Figure 3. Fractures propagated through to bolts F7 and F8 but not to bolts F1 and F3. The varying sizes of shotcrete blocks generated by the shotcrete layer's fracture process likely caused the load to be applied off-centre on the bolt plate and nut, which transferred load to the bolt. Figure 4 shows the deformation of the plate for centre bolt F5, which suggests excentric loading resulting in some shear loading of the bolt instead of pure tension. In contrast, tests LR1 and LR2, without a shotcrete layer, allowed the block to impact on the bolt plate more centrally and applying a more direct tension force, although some slight excentric loading was still possible.

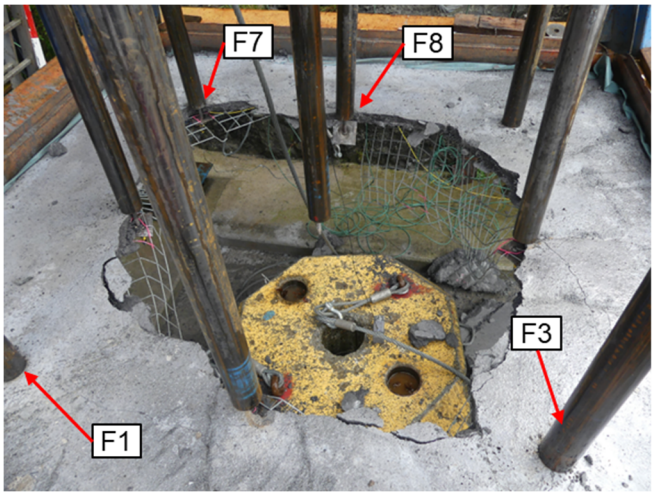

Figure 3 Final shotcrete layer fracture propagation around the dropped block during test LR4, showing fractures through dislodged bolts F7 and F8 while bolts F1 and F3 remain unaffected

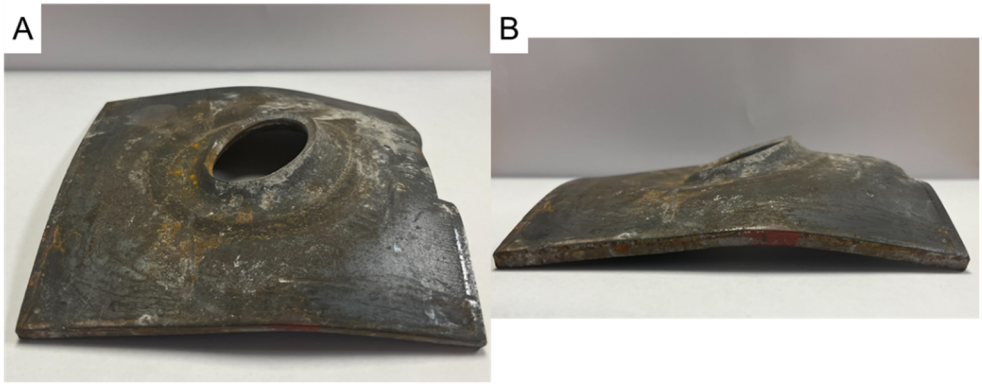

Figure 4 Deformation of the 10-ton dome plate on centre bolt F5 during test LR4. The uneven plate deformation suggests a slight rotation or shear load application on the nut

These observations highlight the complexity of dynamic loading imposed on the ground support scheme at the surface of an excavation. During a seismic event, the dynamic load induced by the sudden bulking and fracturing of the rock mass is transferred from the rock to the plate, which then transfers the dynamic load to the bolt and the surface support. It is reasonable to expect that in some cases, displacements of the fractured rock mass or wedges (represented here by the broken thick shotcrete blocks) can result in combined shear and tension loads on the bolt plate, and consequently on the bolt itself, leading to premature failure.

Figure 2c shows the effect of the shotcrete shell on the load redistribution during phase A. As long as the centre bolt F5 is effective, the stiff shotcrete layer transfers loads to peripheral bolts. As the shotcrete layer fractures it loses its ability to redistribute load to the peripheral bolts. This is recorded by a sharp drop in the loads at each peripheral bolt during or shortly after phase A.

4.1.2 Phase B (30 to 126 ms): load transfer to surface support system and WWM central sheet failure

As soon as the reinforcement system failed at t = 30 ms the fracture propagation in the shotcrete layer continued, reducing the load on the peripheral bolts while the load applied to the surface support system increased. The load was primarily transferred to the mesh strap which is attached to bolts F3 and F7.

In tests LR1 to LR3, which were conducted without shotcrete, it was observed that after the failure of the reinforcement system the peripheral bolts displaced toward the centre as the mesh deformed. This resulted in a plateau in the energy dissipation curve before the surface support system was loaded again as the falling

block moved down. These peripheral bolt displacements were attributed to the inadequate steel tube fixation of the peripheral bolts' installation set-up. However, in this test with the shotcrete layer the bolts were 'locked' in place and did not displace inward. The acceleration curve in Figure 2b shows that the surface support system tended to take the load almost immediately after the reinforcement system failed. This is supported by the acceleration curve that stayed above 0 g, indicating deceleration of the block.

Most of the load was transferred to the mesh strap as it is the stiffer element of the surface support system. However, as the shotcrete layer became more fractured, some peripheral bolts attached to the mesh strap (such as F7) were dislodged and experienced displacement toward the falling block, no longer restricted by the shotcrete. This is shown in Figure 5a, presenting the position of bolt F7 at t = 30 ms, and Figure 5b, showing the previous position of F7 at t = 30 ms and its displacement at t = 126 ms. This displacement of bolt F7 allowed more deformation of the mesh strap and transferred part of the load to the WWM attached to bolts F2, F4, F6 and F8.

At around t = 80 ms the wires and welds of the WWM centre sheet attached to bolt F2 broke. At around t = 108 ms the wires and welds attached to bolt F4 broke, quickly followed by those around bolt F8. By t = 126 ms the last wires attached around bolt F6 broke, indicating that the WWM centre sheet had failed, and the load was fully transferred to the mesh strap and peripheral bolts F3 and F7.

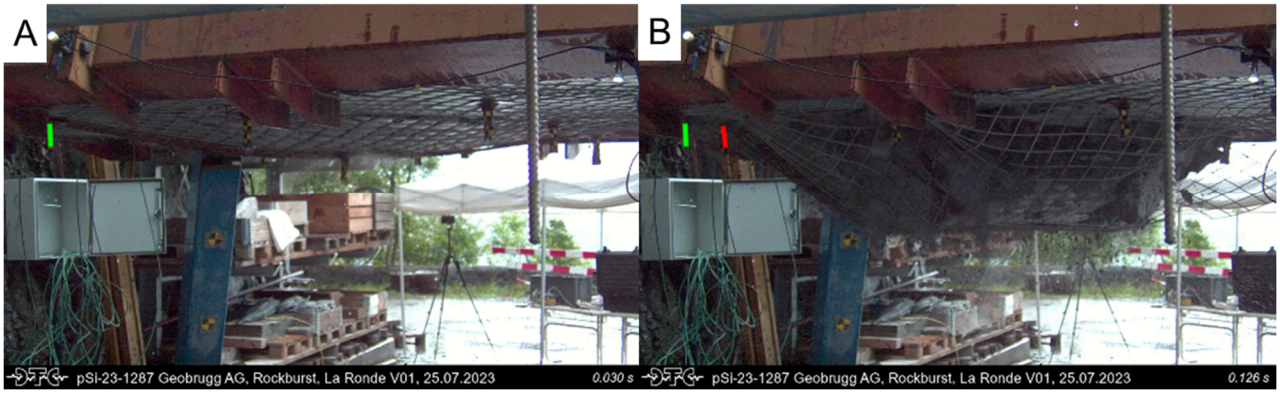

Figure 5 Position and displacement of the head of bolt F7 during test LR4: (a) Position of bolt F7 at t = 30 ms in green, showing initial conditions post-reinforcement system failure; (b) Displacement of bolt head F7 from its position at t = 30 ms in green to its new position at t = 126 ms in red, illustrating the extent of lateral movement and the resulting deformation of the mesh strap at t = 126 ms

4.1.3 Phase C (126 to 202 ms): progressive failure of the mesh strap and the surface support system

After the failure of the WWM central sheet the load was redistributed to the mesh strap and the attached peripheral bolts F7 and F3. While bolt F3 did not show significant displacement due to minimal shotcrete fracturing around it, bolt F7 continued to displace until it tensioned at around t = 156 ms. At this point, as shown in Figure 2c, the load on F7 increased. Supported by video analysis, this increase indicated that a large shotcrete block was redistributing the load from the falling block onto bolt F7, also exerting additional tension on the mesh strap attached to it. The combined effect of the mesh strap tension on the bolt plate and the shotcrete block created a moment force on the bolt's plate, resulting in bending of the bolt as shown in Figure 6.

During this phase the mesh strap wires and welds around F7 gradually broke, eventually reaching failure around t = 202 ms, with a maximum recorded load on F7 peaking at 68.8 kN. Following the failure of the mesh strap at t = 202 ms, the block experienced rotation and increase in acceleration, suggesting that the surface support system was fully consumed. This was supported by the return to –1 g acceleration in Figure 2b, signifying the block's return to a freefall state. The LR4 ground support scheme dissipated a total of 116 kJ over a total displacement of 0.66 m at t = 202 ms. However, it was significantly damaged prior to this point.

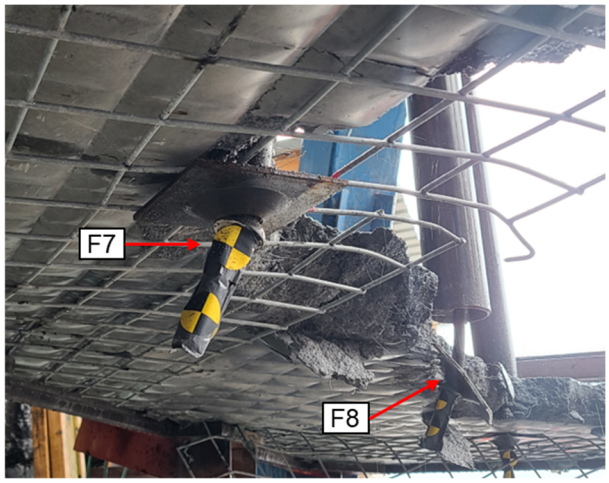

Figure 6 Bending of bolt F7 caused by the tension from the mesh strap and the moment force exerted on the bolt's nut

4.2 Configuration LR5

Figure 7 presents the results for dynamic testing configuration LR5. In this configuration, a 10 cm layer of poured steel-fibre shotcrete covered the surface support system, which consists of high-tensile-strength woven mesh M8046. The reinforcement system includes a 22 mm rebar with a 10-ton dome plate in a continuous tube as central bolt F5. Figure 7 also illustrates key steps in the progressive failure process that are marked by vertical lines at specific time intervals, defining the phases of failure as described below.

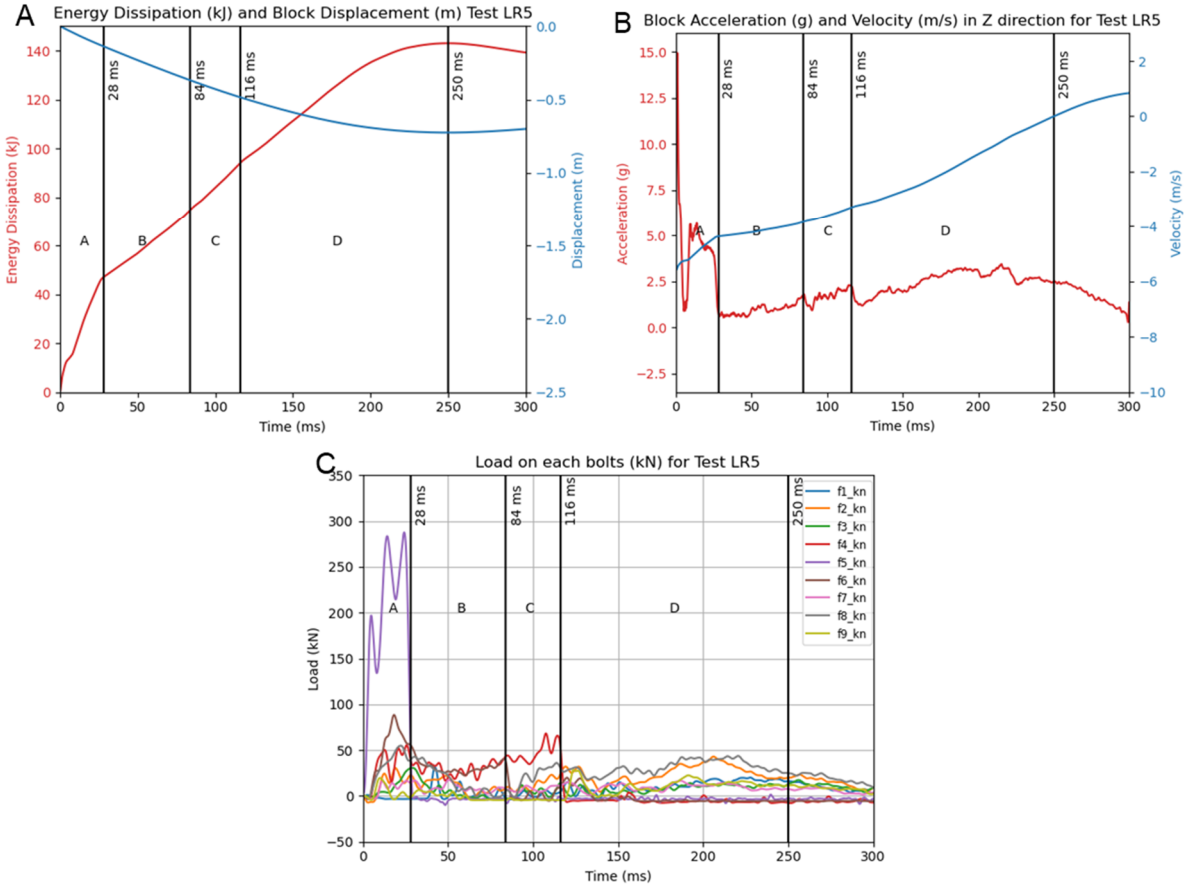

Figure 7 Results and data visualisation for testing configuration LR5: (a) Block displacement (m) and energy dissipation during impact; (b) Block acceleration (g) and velocity (m/s) during impact; (c) Bolt load distribution during impact

4.2.1 Phase A (0 to 28 ms): initial impact, shotcrete layer fracture propagation and reinforcement system response

From 0 to 4 ms the shotcrete is fractured first. This causes a deceleration of the falling block at impact as shown in Figure 7a. The 10-ton dome plate begins to deform. After the plate deforms the load is transferred to the rebar until the plate deforms enough to pass over the nut, as was observed in tests LR1 and LR2 (Durham et al. 2024). This indicates incompatibility with the plate capacity and inefficient load transfer to the bolt due to the weak plate. Beyond t = 28 ms the failure of the reinforcement system initiates the redistribution of the load to the surface support system attached to the peripheral bolts and the rig. As discussed in test LR4, the shotcrete layer helps to redistribute the load to the peripheral bolts early in the fracturing process but this effect diminishes as the thick shotcrete layer continues to fracture (as illustrated in Figure 7c) due to the decrease in load in the peripheral bolts.

4.2.2 Phase B (28 to 84 ms): load transfer to the surface support system and mesh wires attached to bolt F6 breaks

By comparison with previous tests without shotcrete as detailed in Durham et al. (2024), the mesh is observed to take on load more quickly with shotcrete than without. The mesh system begins to redistribute the load to the peripheral bolts after the central bolt fails at t = 28 ms. Due to the woven wire mesh configuration and its load redistribution characteristics, described in Durham et al. (2024), the loads are concentrated at the ends of the rhomboidal shapes of the mesh which are attached to bolts F4 and F6. At t = 84 ms the load on the mesh attached to bolt F6 reaches the strength limit of the wire, with the load peaking at about 40.4 kN (as observed in Figure 7c). This peak was quickly followed by a sharp drop in load, indicating that the wire mesh around F6 had broken.

4.2.3 Phase C (84 to 116 ms): load redistribution on mesh wire attached to bolt F4 and ruptures

Following failure of the wires attached to F6 the load on the mesh shifted to the wires attached to bolt F4, located on the opposite side, and to the rig further away from the falling block. An increase in load on F4 is visible in Figure 7c, peaking at 68.2 kN before a sharp drop at t = 116 ms, indicating the failure of the mesh wires attached to F4.

4.2.4 Phase D (116 to 250 ms): progressive load redistribution and partial failure of the mesh until the block is fully contained

After the failure of the mesh attached to bolts F4 and F6 at t = 116 ms, the load is redistributed in the mesh to the peripheral bolts and the rig, as observed in Figure 7c. As shown in Figure 7b, the block is progressively decelerated, redistributing the dynamic load in the surface support system until the block is fully contained and comes to rest at t = 250 ms. At this point, the maximum energy dissipated by the system was 143 kJ with a maximum displacement of 0.73 m. Since the block is fully contained by the ground support at t = 250 ms due to the configuration of the testing rig and the woven mesh configuration, the block's state of motion after t = 250 ms is comparable to a spring effect and is considered irrelevant for this analysis.

4.3 Configuration LR6

This subsection presents details of the analysis of the results derived from dynamic testing configuration LR6. In this configuration, a 10 cm layer of poured steel-fibre shotcrete covers the surface support system, which consists of a high-tensile-strength woven mesh M8046. The reinforcement system includes a 22 mm rebar with a G-Plate in a continuous tube as central bolt F5. Figure 8 illustrates data visualisation and key steps in the progressive failure process that are marked by vertical lines at specific time intervals, defining the phases of failure as described below.

4.3.1 *Phase A (0 to 24 ms): initial impact, shotcrete layer fracture propagation and reinforcement system response*

This phase covers the initial impact, the initiation of fracturing in the shotcrete layer and the response of the reinforcement system, which comprises a 22 mm rebar with a G-Plate instead of a 10-ton dome plate. The block impacts the shotcrete layer first, inducing a deceleration of the block and initiating fracture propagation in the shotcrete layer, creating shotcrete blocks of various sizes under and around the falling block. The G-Plate successfully transferred the load to the central bolt, which failed at the threads at t = 24 ms after sustaining a maximum load of 327.6 kN, as shown in Figure 8c. As observed in tests LR4 and LR5, and illustrated in Figure 8c, the shotcrete layer tends to redistribute some load to the peripheral bolts early in the failure process. This load redistribution appears to attenuate as the shotcrete fracture propagation intensifies.

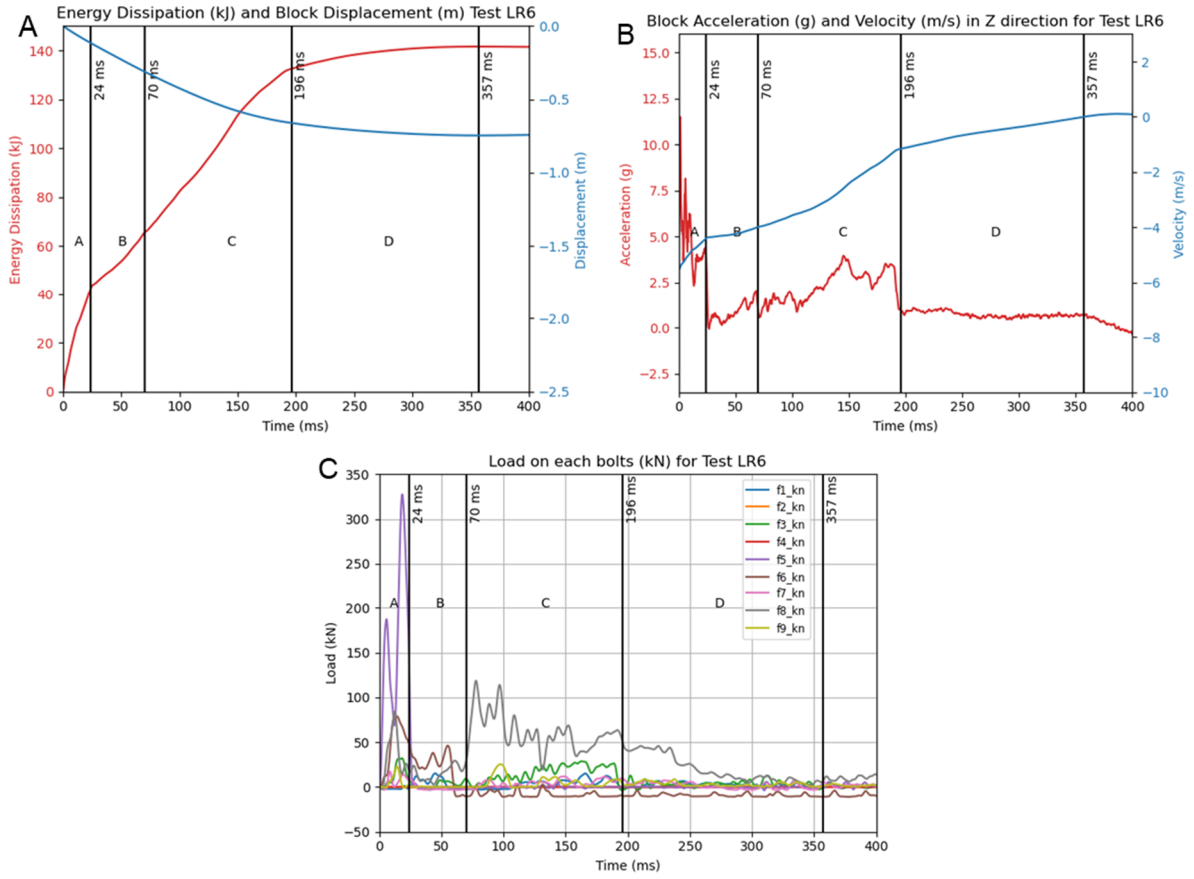

Figure 8 Results and data visualisation for testing configuration LR6: (a) Block displacement (m) and energy dissipation during impact; (b) Block acceleration (g) and velocity (m/s) during impact; (c) Bolt load distribution during impact

4.3.2 *Phase B (24 to 70 ms): surface support system load transfer and rupture of mesh wires attached to bolts F4 and F6*

Figure 8b illustrates the reinforcement system failure with a sharp drop of around t = 24 ms. The load is quickly redistributed across the surface support system. This redistribution results in a noticeable slope increase in the acceleration curve of the block. The load on the woven wire mesh is concentrated primarily at the ends of the rhomboidal shapes of the mesh attached to bolts F4 and F6. At approximately t = 56 ms, the load on the mesh near bolt F6 reaches its strength limit. Figure 8c shows that the load on F6 peaks at about 46.2 kN. This peak is immediately followed by a sharp drop in load, indicating the rupture of the wires around F6. Due to a malfunction in the load cell on F4, load data for F4 is unavailable. However, Figure 8b shows a variation in the block acceleration at t = 70 ms, suggesting that the wires around F4 also broke.

This observation aligns with video analysis, corroborating the timing and sequence of the load transfer and wire rupture events.

4.3.3 Phase C (70 to 196 ms): load redistribution in the surface support system to the peripheral bolts and rig, and partial failure of the mesh

Following the opening in the mesh created by the mesh wires' damage around bolts F4 and F6, the load is redistributed to the peripheral bolts and the rig to which the wire mesh is attached. This results in progressive failure of the mesh, as evidenced by variations in acceleration from t = 70 ms to t = 196 ms. By t = 196 ms an opening in the mesh has formed, located across the opening created by the failure of the wires around bolt F6 at t = 56 ms (as illustrated in Figure 9), and induced a rotation of the falling block towards bolts F1, F2 and F3. Most of the energy was dissipated during this phase of the failure process.

As shown in Figure 8c, bolt F8 appears to carry load after the failure of the mesh wires around F4 and F6, indicating that the load is redistributed to peripheral bolts. The increased tension in the mesh around F8 might also be attributed to fractured shotcrete blocks and the proximity of the corner of the falling block to the F8 plate. Both the shotcrete blocks of various sizes and the falling block increase the tension in the mesh and affect the load on this bolt, as illustrated in Figure 10. The load gradually decreases after the opening created at t = 196 ms appears on the other side of the block, near F1 and F2, as shown in Figure 9.

4.3.4 Phase D (196 to 357 ms): progressive attenuation of the load redistribution and block fully contained by the surface support system

After the mesh experiences the last significant failures at t = 196 ms the block begins to decelerate gradually. The surface support system successfully contains the block at t = 357 ms, dissipating a maximum energy of 142 kJ and reaching a maximum displacement of 0.75 m. Due to the configuration of the testing rig, the state of motion of the block beyond t = 357 ms is comparable to a spring effect and is considered irrelevant for this analysis.

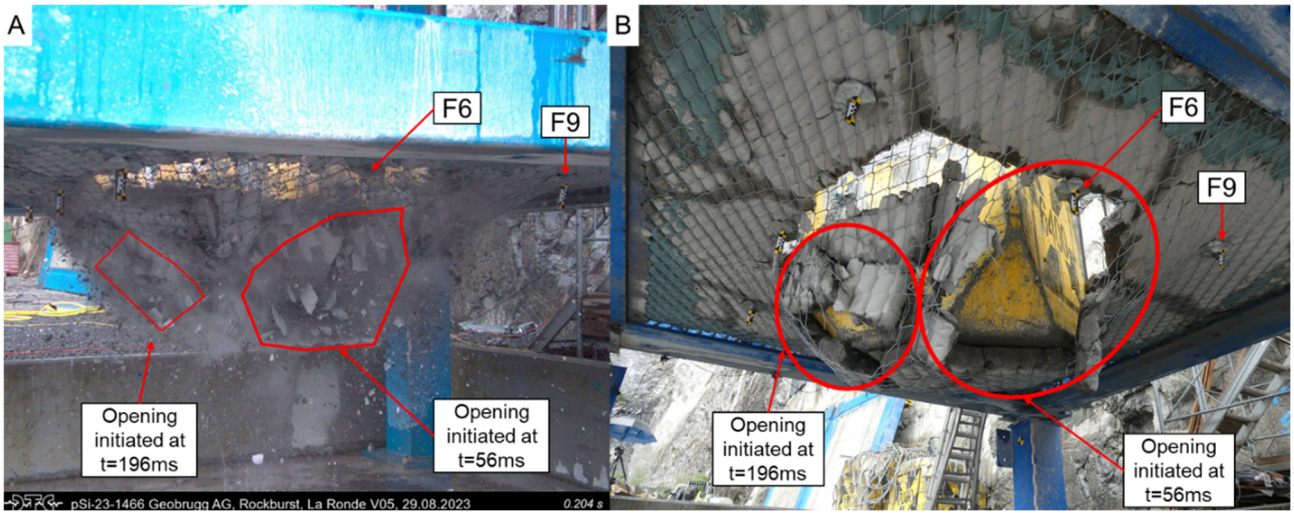

Figure 9 Illustration of the holding capacity of the damaged mesh. The damage initiated around bolt F6 at t = 56 ms and near the corner of the mass around t = 196 ms. The figure shows two snapshots: (a) At t = 204 ms, capturing the progression of the opening; (b) At the end of the test, showing the extent of the mesh damage

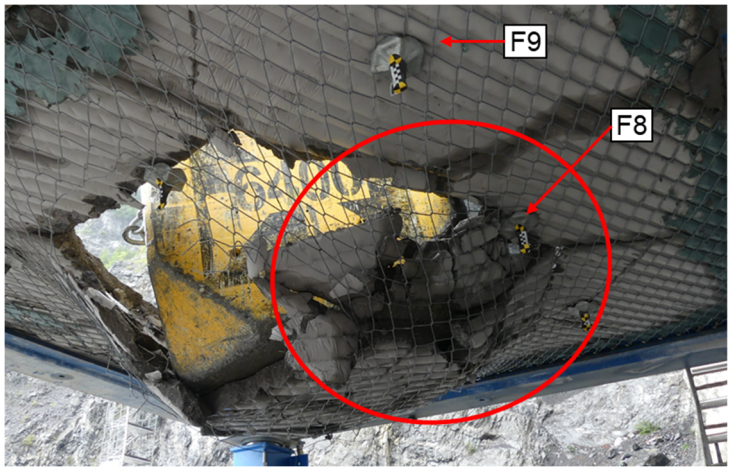

Figure 10 The mass is contained by the ground support scheme in test LR6. The photo shows the fractured shotcrete blocks and the corner of the mass near the F8 plate

4.4 Configuration KI1

This subsection presents details of the analysis of the results derived from dynamic testing of the KI1 configuration, where the reinforcement system middle bolt F5 is a cement-grouted D-Bolt 22 mm with a G-Plate in a split tube and the mesh system type is a high-tensile-strength woven mesh M8040, which is a smaller grade mesh than the previously tested M8046 woven mesh. Figure 11 illustrates data visualisation and key steps in the progressive failure process that are marked by vertical lines at specific time intervals, defining the phases of failure as described below.

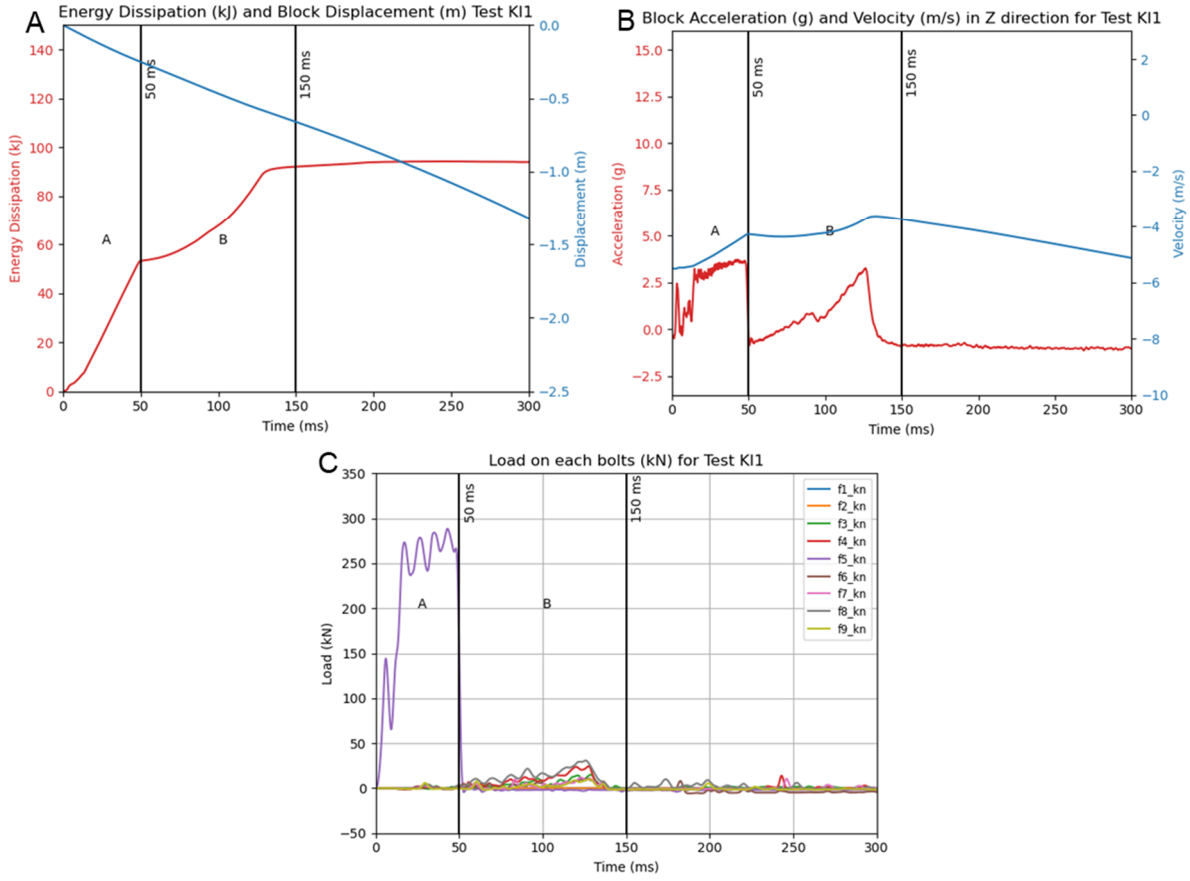

Figure 11 Results and data visualisation for testing configuration KI1: (a) Block displacement (m) and energy dissipation during impact; (b) Block acceleration (g) and velocity (m/s) during impact; (c) Bolt load distribution during impact

4.4.1 Phase A (0 to 50 ms): initial impact and reinforcement system response

This phase covers the initial impact of the block and the response of the reinforcement system, which consists of a cement-grouted D-Bolt with a G-Plate installed within a split tube configuration to facilitate debonding. The set-up successfully transferred the load to the bolt, leading to debonding of the bolt and its subsequent failure.

The G-Plate thickness is approximately 0.045 m (Geobrugg 2013). The plate initially deforms between t = 0 to 8 ms, dissipating about 4 kJ of energy before transferring the load to the bolt. However, because of the testing set-up, a square steel plate was installed under the mesh, as shown in Figure 1d. The diameter of this plate is smaller than the diameter of the D-Bolt nut. Therefore it is not possible to properly interpret the load transfer from the G-Plate to the bolt as the square plate under the mesh has likely contributed to this load transfer.

The bolt reached a peak load of 288 kN (averaging about 265 kN) before the head of the bolt ruptured at the threads at t = 50 ms. Additionally, the yielding section of the bolt, visible at the split of the tube, stretched by 0.125 m, demonstrating the bolt's yielding capability. This phase highlights the dynamic bolt's ability to undergo significant deformation, thereby working to dissipate substantial energy before failure as compared to a stiffer bolt such as a resin-grouted rebar. At the time of bolt failure, t =50 ms, the reinforcement system exhibited a maximum displacement of 0.25 m and dissipated 53 kJ.

4.4.2 Phase B (50 to 150 ms): load transfer and progressive failure of the surface support system

As the central bolt stretched from t = 0 to 50 ms the mesh deformed, but there is no load on the peripheral bolts. Figure 11b shows that after the failure of the reinforcement system at t = 50 ms the block's acceleration approached –1 g, suggesting a near freefall state for a short period of time (<5 ms). At t = 50 ms the data indicates a redistribution of the loads through the mesh to the peripheral bolts and rig. The load is concentrated on the ends of the rhomboidal shapes of the woven wire mesh attached to bolts F2 and F8. In Figure 11c it is possible to observe the slower increase of load in bolt F8 compared to previous tests using the stronger M8046 woven mesh. The load cell on F2 malfunctioned on this test. Video analysis shows tension in the mesh resulting in a progressive failure of the mesh initiating under the block, particularly beneath the centre bolt F5, following the failure of the reinforcement system at t = 50 ms. This suggests that the mesh was damaged during the impact and during phase A when the reinforcement system was loaded by the square plate under the mesh. The wires of the mesh attached to bolts F8 and F2 did not break compared to previous tests using the M8046 mesh.

The opening in the mesh progressively increased as wires ruptured from the centre through to the peripheral bolts F8 and F2, until the block fell through around t = 150 ms. At this point the acceleration returned to –1 g, indicating a freefall state as shown in Figure 11b. The ground support scheme of the K1 configuration dissipated a total of 92 kJ over a total displacement of 0.66 m.

5 Discussion

Based on the comprehensive analysis of the four test configurations (LR4, LR5, LR6, KI1) described in the previous sections and the three configurations (LR1, LR2, LR3) detailed in Durham et al. (2024), the process of energy dissipation and the failure mechanisms within the ground support schemes can be described as follows:

1. The central bolt of the reinforcement system dissipates energy up to the point of failure, either of the plate or the bolt.
2. Concurrently with the application of loads on the reinforcement system, the surface support system undergoes limited deformation. When the central bolt fails the mesh is tensioned, initiating the redistribution of loads across the surface support system and onto the peripheral bolts. The amount of tension prior to bolt failure depends on the bolt stretch but is not significant compared to the tension induced post-failure. The load transfer via the surface support system to the peripheral bolts depends on the stiffness of the support.

3. The failure of the mesh system initiates at localised points of concentrated load, typically in the wires around the attachment points to the side bolts. This is where the concentration of dynamic loads leads to the initial breakdown of the mesh, which creates openings in the mesh system. This marks the beginning of its failure.
4. Following the localised failure of the mesh at points of restraint and opening, the load is then redistributed to bolts located further from the initial impact. This leads to a progressive weakening and the eventual collapse of the mesh system, indicating the failure of the ground support scheme.

A comparative table of the results from the seven dynamic tests conducted in this program is presented in Table 2. This table highlights the testing configuration characteristics, and the performance of the reinforcement systems and ground support schemes at failure or when the falling block was contained.

In each test involving shotcrete (LR4, LR5, LR6) it was noted that the fracturing of the shotcrete and the resulting shotcrete blocks significantly influences the failure mechanisms of the ground support scheme during dynamic testing. At the time of impact the shotcrete layer helps to decelerate the falling block more rapidly, as shown in Table 2. The stiffer surface support redistributes the load to the peripheral bolts as the shotcrete remains relatively unfractured during the initial reinforcement system response (phase A). As the reinforcement system reaches failure, the fracture propagation within the shotcrete intensifies, preventing further load redistribution due to the extensive fracturing. Once the shotcrete is fractured enough it may dislodge bolts, no longer preventing lateral displacement. Based on the full suite of results it was observed that the shotcrete layer tends to add variability to the tests, reducing comparability between tests of different configurations.

These tests can be seen as a proxy for ground support and rock mass blocks interaction. The tests illustrate the complexity of damage mechanisms and how the fractured rock blocks may interact with the surface support and the reinforcement system. The tests also demonstrate this complexity, showing that rock blocks can punch through the mesh, bolts can be subjected to both shear and tension forces, or bolts can be dislodged at the head, experiencing lateral displacement as observed.

It is noteworthy that tests LR5 and LR6 managed to contain the falling blocks with similar maximum dissipated energy (LR5 at 143 kJ and LR6 at 142 kJ) and similar results in general. This demonstrates the consistency of the testing set-up and approaches. However, since these two tests were conducted on testing rig 2 with a testing surface of 4 × 4 m while the other tests were conducted on rig 1 with a 3.6 × 3.6 m surface, the lack of documentation on the differences between the rigs prevents us from concluding that they contributed significantly to the results observed in tests LR5 and LR6. Tests LR5 and LR6, using WWM M8046, outperformed test LR4, which used mesh straps and WWM sheets. However, since a different rig was used for LR4, and the mesh and mesh strap arrangement was not optimal, it is not possible to conclude with confidence the performance of the mesh strap configuration. More tests are needed to better evaluate the rig's contribution to the testing results and improved installation of the mesh and mesh straps. The performance of the G-Plate compared to the 10-ton dome plate appears marginally better in terms of load transfer to the bolt, based on the results of LR5 and LR6, but other performance metrics are similar or lower.

The performance of the cement-grouted 22 mm D-Bolt with a G-Plate used in the KI1 test was superior to the 22 mm PAR1 with 21-ton dome plates used in the LR3 test. In test LR3, the dynamic performance of the PAR1 resulted in a maximum displacement of 0.18 m, an energy dissipation of 40 kJ and a debonding length between the two sets of paddles of ΔL = 0.068 m. Given that the distance between the two sets of paddles of the PAR1 bolt is L_0 = 1.1 m, the strain S experienced by the bolt in test LR3 is $S = \frac{\Delta L}{L_0}$ = 6.2%. In comparison, the D-Bolt reinforcement system in test KI1 demonstrated a maximum displacement of 0.25 m, an energy dissipation of 53 kJ and a debonding length of ΔL = 0.125 m between its paddles. The D-Bolt in test KI1 features three sets of paddles with a distance of L_0 = 0.9 m between each set, compared to the PAR1, which has only two sets of paddles. Therefore the strain for the D-Bolt in test KI1 is calculated as $S = \frac{\Delta L}{L_0}$ = 14%. The potential reasons for this difference may be that the PAR1 is resin-grouted, making it stiffer than the cement-grouted D-Bolt used in test KI1 (Villaescusa et al. 2023). Alternatively, or in combination, there may

be differences in the steel properties or variations in the paddle configuration. Single bolt tests would be needed to draw more definitive conclusions.

Table 2 Reinforcement and ground support systems' dynamic performance comparison table

Test ID	LR1	LR2	LR3	LR4	LR5	LR6	KI1
Rig	R1	R1	R1	R1	R2	R2	R1
Mesh system type	WWM	M8046	M8046	WWM + mesh strap	M8046	M8046	M8040
Shotcrete	No	No	No	10 cm FRS	10 cm FRS	10 cm FRS	No
Bolting pattern	1.4 × 1.4 m + centre	1.4 × 1.4 m + centre	1.4 × 1.4 m + centre	1.4 × 1.4 m + centre	1.4 × 1.4 m + centre	1.4 × 1.4 m + centre	1.2 × 1.2 m
Reinforcement bolt type (F5)	Rebar 22 mm	Rebar 22 mm	PAR-1 22 mm	Rebar 22 mm	Rebar 22 mm	Rebar 22 mm	D-Bolt 22 mm
Bolt plate	10-ton dome	10-ton dome	21-ton dome	10-ton dome	10-ton dome	G-Plate	G-Plate
Split tube	No	No	Yes	No	No	No	Yes
Reinforcement system performance (Phase I)							
Reinforcement system failure at t (ms)	14	14	34	30	28	24	50
Element failed	Plate	Plate	Bolt	Bolt	Plate	Bolt	Bolt
Peak dynamic load on reinforcement element (kN)	182.5	194.5	311.4	310.7	287.6	327.6	288.5
Maximum displacement before failure (m)	0.08	0.08	0.18	0.14	0.14	0.11	0.25
Maximum loading mass deceleration (g)	2.3	2.6	4.3	9.8	14.9	11.5	3.71
Energy dissipated by reinforcement system (kJ)	8	6	40	61	47	43	53
Ground support scheme performance							
Maximum displacement before failure (m)	0.91	1.32*	0.80	0.66	0.73	0.75	0.66
Maximum energy dissipated by ground support scheme (kJ)	39	103*	83	116	143	142	92
System failure	Fail	Fail	Fail	Fail	Contain	Contain	Fail

* The high-energy dissipated and maximum displacement reported in this test are misleading as the block was temporarily retained by the mesh that formed a 'rope' around the block, as explained in Durham et al. (2024).

It is also possible to compare the performance of the surface support systems in the LR3 and KI1 test configurations. The LR3 test used a woven wire mesh M8046 made of 4.6 mm grade wire whereas the KI1 test used a mesh M8040 made of 4.0 mm grade wire, which is less strong. Despite the M8040 mesh being weaker, the overall ground support scheme in the KI1 test configuration demonstrated superior performance compared to the LR3 test. This further highlight the contribution of the D-Bolt, which outperformed the PAR1 in the energy dissipation capacity of the KI1 configuration. However, the KI1 test allowed less maximum displacement before complete failure, with a maximum displacement of 0.66 m compared to 0.8 m in the LR3 test.

It must be noted that the maximum energy dissipation values provided in Table 2 do not represent design capacities. The test program was initiated to investigate and study the combined performance of reinforcement and support systems but not as a proof test of specific ground support schemes. Repeated tests of a particular configuration would be needed to define design capacities.

6 Conclusion

In a collaborative effort between Geobrugg and the LaRonde and Kittilä mines, a large-scale laboratory testing program was initiated in May 2023 to research avenues for enhancements and innovation in the dynamic energy dissipation capabilities of ground support schemes. The testing program was conducted at the Walenstadt Geobrugg testing facility. The sophisticated set-up at the facility, instrumentation and analytical methodologies developed were utilised to measure the dynamic responses and analyse the energy dissipation performance of seven distinct ground support configurations. Testing configurations LR1, LR2 and LR3 were analysed in Durham et al. (2024), and LR4, LR5, LR6 and KI1 were detailed in this paper. A thorough analysis of each test configuration was conducted using comprehensive data analysis and video interpretation. The analysis methodology detailed in Durham et al. (2024) provides a consistent framework for describing the behaviour and response to dynamic loading of each testing configuration, and the limitations of each tested configuration are identified. This approach ensures that the observed outcomes accurately align with the recorded data.

The tests conducted with shotcrete can be seen as a proxy for ground support and rock mass blocks interaction. The tests illustrate the complexity of damage mechanisms and how the fractured rock blocks may interact with surface support and the reinforcement system. The tests also demonstrate this complexity, showing that rock blocks can punch through the mesh, bolts can be subjected to both shear and tension forces, or bolts can be dislodged at the head, experiencing lateral displacement (as observed).

Testing with the mesh and mesh strap was unfortunately not conclusive, however, the performance of the high-tensile-strength woven mesh was good when combined with yielding bolt (LR3). This is attributed to its intricate interwoven wire structure and rhomboidal geometry. This design efficiently dissipates energy across multiple wires near the load area and concentrates load at the rhomboidal ends, unlike the overlapped WWM which relies on welds for load redistribution, impacting overall energy dissipation within the surface support system.

The goal of this project was to advance the understanding of the energy dissipation and deformation capacity of ground support schemes for improved performance under demanding dynamic conditions. The key takeaway from these tests underscores the importance of not only the strength of individual components within the ground support system but also the strategic arrangement of these elements to optimise energy dissipation under dynamic conditions. Future work is required to address some of the limitations and variability raised during this test program.

7 Acknowledgment

The authors are grateful to Agnico Eagle Mines for permission to publish this paper. The collaboration between the personnel of Agnico Eagle and Geobrugg is gratefully acknowledged. The Walenstadt site team, Mr Kamal Khodja and Mr Johan Persson are appreciated for their technical contributions and support.

References

Brändle, R & Luis Fonseca, R 2019, 'Dynamic testing of surface support systems', in J Hadjigeorgiou & M Hudyma (eds), *Ground Support 2019: Proceedings of the Ninth International Symposium on Ground Support in Mining and Underground Construction*, Australian Centre for Geomechanics, Perth, pp. 243–250, https://doi.org/10.36487/ACG_rep/1925_15_Brandle

Brändle, R, Rorem, E, Luis, R & Fischer, G 2017, 'Full-scale dynamic tests of a ground support system using high-tensile strength chain-link mesh in El Teniente mine, Chile', in M Hudyma & Y Potvin (eds), *UMT 2017: Proceedings of the First International Conference on Underground Mining Technology*, Australian Centre for Geomechanics, Perth, pp. 25–43, https://doi.org/10.36487/ACG_rep/1710_01_Luis

Doucet, C & Voyzelle, B 2012, technical information data sheets, CanmetMINING, Ottawa.

Durham, C, Falmagne, V, Caron, M-E & Brändle, R 2024, 'Experimental assessment of the energy dissipation and deformation capacity of ground support systems under dynamic loading: insights from LaRonde mine dynamic drop test program', *Proceedings of the 58th U.S. Rock Mechanics/Geomechanics Symposium*.

Epiroc 2024, *PAR1 Resin Bolt*, viewed 25 April 2024, https://www.epiroc.com/en-ca/products/rock-drilling-tools/ground-support/energy-absorbing-rockbolts/par1-resin-bolt

Geobrugg 2013, *G-Plate GS-8079—Untertage Krallplatte USP 15/40 fur G80- Drawing Sheet*.

Kaiser, PK, McCreath, DR, Brummer, RK, Maloney, S, Vasak, P & Xiaoping, Y 1996, *Canadian Rockburst Support Handbook*, Geomechanics Research Center, Sudbury.

Knox, G & Hadjigeorgiou, J 2022, 'Influence of testing configuration on the performance of paddled energy-absorbing rockbolts under impact loading', *Rock Mechanics and Rock Engineering*, vol. 55, no. 9, pp. 5705–5721, https://doi.org/10.1007/s00603-022-02945-1

Normet 2024, *Normet D-Bolt®—Dynamic Bolt*, viewed 17 May 2024, https://www.normet.com/en/products-and-services/rock-reinforcement/dynamic-bolts/normet-D-Bolt/

Ortlepp, WD & Stacey, TR 1994, 'Rockburst mechanisms in tunnels and shafts', *Tunnelling and Underground Space Technology*, vol. 9, no. 1, pp. 59–65, https://doi.org/10.1016/0886-7798(94)90010-8

Potvin, Y & Hadjigeorgiou, J 2020, *Ground Support for underground mines*, Australian Centre for Geomechanics, Perth.

Roth, A, Cala, M, Brändle, R & Rorem, E 2014, 'Analysis and numerical modelling of dynamic ground support based on instrumented full-scale tests', in M Hudyma & Y Potvin (eds), *Deep Mining 2014: Proceedings of the Seventh International Conference on Deep and High Stress Mining*, Australian Centre for Geomechanics, Perth, pp. 151–163, https://doi.org/10.36487/ACG_rep/1410_08_Roth

Sasseville, G, Turcotte, P & Falmagne, V 2022, 'Control measures to manage seismic risk at the LaRonde mine, a deep and seismically active operation', *Proceedings of the 56th U.S. Rock Mechanics/Geomechanics Symposium*, American Rock Mechanics Association, Alexandria, https://doi.org/10.56952/ARMA-2022-0625

Vallejos, JA, Marambio, E, Marulanda, Y, Burgos, L & Gonzalez, C 2019, 'Progress in the numerical modelling of dynamic testing for reinforcement and retaining elements used in underground excavations', in J Hadjigeorgiou & M Hudyma (eds), *Ground Support 2019: Proceedings of the Ninth International Symposium on Ground Support in Mining and Underground Construction*, Australian Centre for Geomechanics, Perth, pp. 357–374, https://doi.org/10.36487/ACG_rep/1925_24_Marambio

Villaescusa, E, Thompson, AG, Windsor, CR & Player, JR 2023, *Ground Support Technology for Highly Stressed Excavations: Integrated Theoretical, Laboratory, and Field Research,* CRC Press, Boca Raton, https://doi.org/10.1201/9781003357711

Windsor, CR & Thompson, AG 1992, 'Reinforcement design for jointed rock masses', *The 33rd U.S. Symposium on Rock Mechanics (USRMS)*, A.A. Balkema, Rotterdam.